LBL-28873
Preprint

Lawrence Berkeley Laboratory
UNIVERSITY OF CALIFORNIA

Materials & Chemical
Sciences Division

Submitted to Journal of Chemical Physics

# Photoelectron Spectroscopy and Electronic Structure of Clusters of the Group V Elements. III. Tetramers: The $^2T_2$ and $^2A_1$ Excited States of $P_4^+$, $As_4^+$ and $Sb_4^+$

L.-S. Wang, B. Niu, Y.T. Lee, D.A. Shirley,
E. Ghelichkhani, and E.R. Grant

June 1990



Prepared for the U.S. Department of Energy under Contract Number DE-AC03-76SF00098.

## DISCLAIMER

LBL-28873

# Photoelectron Spectroscopy and Electronic Structure of Clusters of the Group V Elements. III. Tetramers: The $^2T_2$ and $^2A_1$ Excited States of $P_4^+$, $As_4^+$ and $Sb_4^+$

L.-S. Wang, B. Niu, Y.T. Lee, and D.A. Shirley
Department of Chemistry
University of California
and
Materials and Chemical Sciences Division
Lawrence Berkeley Laboratory
University of California
Berkeley, CA 94720

and

E. Ghelichkhani and E.R. Grant
Department of Chemistry
Purdue University
West Lafayette, IN 47907

This work was supported by the Director, Office of Energy Research, Office of Basic Energy Sciences, Chemical Sciences Division of the U.S. Department of Energy under Contract No. DE-AC03-76SF00098, by the National Science Foundation through Grant No. CHE-8920555, and by the Alexander von Humboldt Foundation through a Senior Scientist Award to DAS.

## Abstract

Methods employing high resolution HeI (584Å) photoelectron spectroscopy, have been applied to the tetrameric clusters of the group V elements, to resolve details of vibronic and spin-orbit structure in the first three electronic states of $P_4^+$, $As_4^+$, and $Sb_4^+$. Measured spacings of distinct vibrational progressions in the $\nu_1$ mode for the $^2A_1$ states of $P_4^+$ and $As_4^+$, yield vibrational frequencies of 577 (5) $cm^{-1}$ for $P_4^+$ and 350 (6) $cm^{-1}$ for $As_4^+$. Franck-Condon factor calculations suggest bond length changes for the ions in the $^2A_1$ states of 0.054 (3) Å for $P_4^+$ and 0.060 (3) Å for $As_4^+$. Strong Jahn-Teller distortions in the $\nu_2(e)$ vibrational mode dominate the structure of the $^2E$ ground states of the tetrameric ions. Both Jahn-Teller and spin-orbit effects appear in the spectra of the $^2T_2$ states of the tetrameric ions, with the spin-orbit effect being dominant in $Sb_4^+$ and the Jahn-Teller effect dominant in $P_4^+$. Vibrational structure is resolved in the $P_4^+$ spectrum, and the $\nu_3(t_2)$ mode is found to be the one principally active in the Jahn-Teller coupling. A classical metal-droplet model is found to fit well with trends in the IPs of the clusters as a function of size.

# I. Introduction

In the preceding paper (Paper II),[1] we reported the high-resolution photoelectron spectra of the homonuclear Group V tetramers. Our analysis emphasized Jahn-Teller effects on the vibronic spectra of the strongly distorted $^2E$ ground states of $P_4^+$, $As_4^+$, and $Sb_4^+$. The first and second excited states of these cations are also well resolved in the photoelectron spectrum. These bands evidence striking contrast in vibronic structure. Thus for all three tetramers, splitting patterns and distributions of spectral intensity vary dramatically in response to electronic configuration. The behavior displayed spans a range from strong Jahn-Teller distortion, to strong spin-orbit splitting, to no vibronic coupling at all. Thus, within this single group of molecules, we find a broad paradigm for a relatively complete set of coupling hierarchies. The present paper surveys overall coupling trends, while considering global properties of the transition of these tetramers to an ionized state. Particularly, we will analyze and discuss the $^2T_2$ and $^2A_1$ excited states in detail.

We begin by briefly reviewing some essential background on Jahn-Teller and spin-orbit coupling and their interaction. We then examine each band system in the photoelectron spectrum of each tetramer from the perspective of its physical significance in terms of these elementary models for the coupling of electronic and internuclear degrees of freedom. We consider implications of the spectra for the geometry of neutrals and various states of the corresponding cations, and we interpret observed ionization thresholds in the light of the classical spherical drop model for cluster electronic structure.

# II. The Jahn-Teller Theorem and the Ham Effect

## *A. The Jahn-Teller Theorem*

The Jahn-Teller theorem[2] states that a nonlinear nuclear framework in a degenerate electronic state (except for the two-fold Kramers degeneracy[3]) is unstable with respect to a first order distortion of the nuclear framework. This instability is caused by a linear

perturbation of the electronic state, which lowers the symmetry of the nuclear framework and lifts the electronic degeneracy. For a nonlinear molecule, this means that the electronic degeneracy forces the potential minimum along a distortion coordinate away from the symmetric position. Thus, a nonlinear molecule in a degenerate electronic state assumes a permanent distortion which produces an observable anisotropy. The Jahn-Teller effect naturally signifies a breakdown of the Born-Oppenheimer approximation separation between vibrational and electronic degrees of freedom, implying unique nonadiabatic dynamics with associated fluxionality.[4] Jahn-Teller effects have been extensively studied,[5] especially in solid-state physics, in investigations of transition metal ions in solid matrices, and impurity atoms or vacancies in crystal lattices.[6] Recent experiments have heightened interest in the Jahn-Teller effect in metal clusters, particularly trimers.[7-9]

### *B. The Ham Effect: Jahn-Teller Effect vs. Spin-Orbit Effect*

In photoelectron spectroscopy, one often starts from a closed-shell molecule with an initial state of spin 0 to produce a final state of spin 1/2. If the ionization proceeds from a degenerate orbital, then the final state with non-zero orbital angular momentum is subject to the spin-orbit effect as well as to the Jahn-Teller effect. These two effects interact and, in a sense, compete to lift the orbital degeneracy. In general, when the two effects are of comparable magnitude, the spin-orbit effect reduces the Jahn-Teller effect. This reduction of the Jahn-Teller effect by the spin-orbit effect is often called the Ham effect.[10] There are two other limits. If the spin-orbit coupling is sufficiently strong, it can stabilize a molecule against Jahn-Teller distortions.[5b,11] On the other hand, when the Jahn-Teller effect is dominant and produces a large distortion, the spin-orbit interaction can be quenched. The $^2T_2$ states in the photoelectron spectra of the current tetramer species span this range of possibilities.

## III. Results and discussion: A survey of vibronic properties and the energetics of photoionization

### *A. The $(1e)^{-1}$ Bands*

The ionization of the 1e orbital results in a $^2E$ term, which is unstable with respect to $\nu_2$ distortion according to the Jahn-Teller theorem. Consequently, two bands are observed, as discussed in Paper II. Figure 1 shows that vibrational structure is partially resolved in the $P_4^+$ spectrum. As given in Table 1, an average vibrational spacing of 315 $cm^{-1}$ is derived for the first band, and 275 $cm^{-1}$ for the second component. These are in agreement with the excitation of the $\nu_2$ mode. As shown in Figures 2 and 3, vibrational structure is barely discernible in the $As_4^+$ spectrum, while none is resolved in the $Sb_4^+$ case, due to their smaller $\nu_2$ vibrational frequencies. From our previous discussion, it is clear that the $\nu_2$ vibrations couple the doubly electronic degeneracy in the $^2E$ term and distort the clusters. Qualitatively, Figure 4 shows the spectral transitions from the ground state to the Jahn-Teller distorted final states. A detailed vibronic calculation on the E⊗e Jahn-Teller problem and the comparison with the experimental results have been presented in Paper II.[1]

### *B. The $(2t_2)^{-1}$ Bands: Jahn-Teller Effect vs. Spin-Orbit Effect*

As can be seen from Figures 1-3, the $(2t_2)^{-1}$ bands are more complicated, and each is composed of three components, which are indicated with Voigt functions in the Figures. The Voigt functions merely serve to show the positions of the three components and to enhance their visibility. Two factors can be attributed to the spectral complexity, the Jahn-Teller effect and the spin-orbit effect. Unlike the $^2E$ state, in the $^2T_2$ term, both the $\nu_2(e)$ and $\nu_3(t_2)$ modes are active in the Jahn-Teller coupling. Moreover, the $^2E$ and $^2T_2$ terms are close to each other in energy, and can have interactions which would further complicate the spectrum.[12]

Clear vibrational structure is resolved for the first component in the $P_4^+$ spectrum, with a vibrational spacing of about 400 $cm^{-1}$, as shown in Figure 1 and Table 1. Compared with the $P_4$ neutral vibrational frequencies, this spacing is larger than the $\nu_2$ frequency, but smaller than the $\nu_3$ frequency. The $2t_2$ MO should be a bonding orbital. Thus, it is reasonable to assign the observed vibrational structure in the $P_4^+$ spectrum to the $\nu_3$ mode. This means that the $\nu_3(t_2)$ mode is the Jahn-Teller active mode in the vibronic interaction while the $\nu_2(e)$ mode may have little involvement. Just the single mode T⊗t Jahn-Teller problem alone is a fairly complicated one. In the present context, we shall restrict ourself only to interpret the qualitative features of the spectra and study the possible Jahn-Teller splittings and the spin-orbit effect, by assuming explicitly a single-mode and single-state problem.

In a $T_d$ point group, the orbital angular momentum of an E term is largely quenched but not for a T term.[6] Therefore, we must consider the spin-orbit effect as well as the Jahn-Teller effect in the $(2t_2)^{-1}$ bands, especially for the $Sb_4^+$ case, where spin-orbit interaction is anticipated to be very important. From Table 1 and Figures 1-3, we see that the splitting between the first and second components in the $(2t_2)^{-1}$ band increases considerably from $P_4^+$ to $Sb_4^+$. For $Sb_4^+$, this splitting is almost the same as the spin-orbit splitting in $Sb^+$, while that in $P_4^+$ is much larger than the spin-orbit splitting in $P^+$. From Figure 3, it is seen that this splitting is the same as that of the $Sb_2^+$ $^2\Pi_u$ spin-orbit splitting, since they overlap almost exactly. Thus, we can account for the splitting between the first and second components in $Sb_4^+$ as being due to the spin-orbit effect, while the splittings in $P_4^+$ should be principally due to the Jahn-Teller effect. Here is an excellent example demonstrating the transition from a strong Jahn-Teller effect in $P_4^+$ to a strong spin-orbit effect in $Sb_4^+$. However, the spin-orbit effect in $P_4^+$ is not negligible. It manifests itself as a result of the Ham effect. It is clear that the Jahn-Teller splitting in the $(2t_2)^{-1}$ bands of $P_4^+$ is significantly smaller than that in the $(1e)^{-1}$ band, strongly suggesting the presence of the Ham effect. That is, the spin-orbit effect suppresses the

Jahn-Teller effect in the $^2T_2$ states. This is, of course, only a qualitative and provisional interpretation. A more quantitative understanding of these complicated spectra will require full theoretical calculations simultaneously treating vibronic interactions, spin-orbit effects, and electron correlation effects.[12]

It is of interest to consider the symmetry of the Jahn-Teller distorted nuclear configurations. As can be seen from Figure 4 in Paper II,[1] the $\nu_3(t_2)$ vibrations tend to distort the $T_d$ $M_4$ molecule toward $C_{2v}$ geometry. Thus, potentials associated with a $^2T_2$ term under strong Jahn-Teller coupling with the $\nu_3(t_2)$ mode should split as follows:[3]

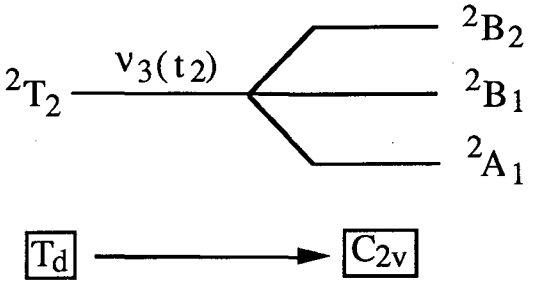


(1)

This should be the case for $P_4^+$, where the Jahn-Teller effect dominates the spin-orbit effect. A schematic representation of the Jahn-Teller splittings based on this scheme is shown in Figure 5(a). This diagram represents a section of the potential energy hyper-surfaces along the $t_2$ distortion coordinate, $\rho$. The potential energy hyper-surfaces have cylindrical symmetry in a harmonic approximation.[6b] The neutral ground state is shown with its vibrational wave function. Franck-Condon transitions from the ground state to the three Jahn-Teller split levels give the observed three components in the $(2t_2)^{-1}$ photoelectron bands. The vibronic level structures are expected to be very complicated at energies above the $^2A_1$ level, which accounts for the lack of vibrational resolution at higher energies beyond the first component.

For $Sb_4^+$, however, a different splitting pattern may be expected, because the spin-orbit effect is dominant. The spin state of a single unpaired electron transforms as $E_{1/2}$ in the $T_d$ point group, and the direct product of $E_{1/2}$ with $^2T_2$ gives the following results:[3]

$$^2T_2 \times E_{1/2} = {}^2E_{5/2} + {}^2G_{3/2} \qquad (2)$$

where the component $^2E_{5/2}$ has no spatial degeneracy (only the two-fold Kramers degeneracy), and the component $^2G_{3/2}$ has two-fold spatial degeneracy and is susceptible to further Jahn-Teller splitting. Thus, the following may be a more appropriate splitting scheme for the adiabatic potentials associated with the $(2t_2)^{-1}$ band of $Sb_4^+$:

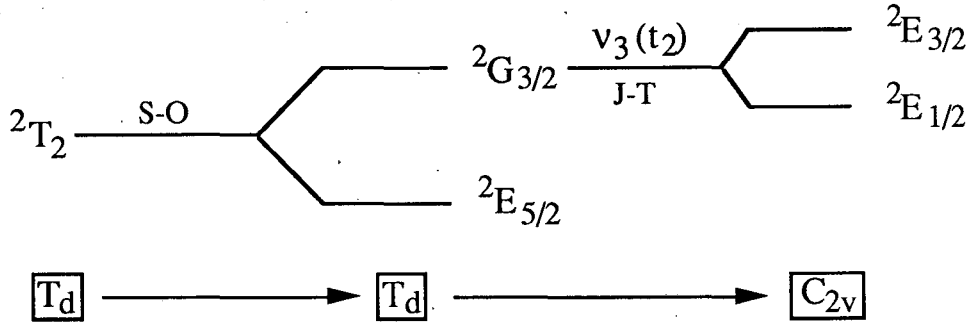


(3)

where S-O stands for the spin-orbit interaction, and J-T the Jahn-Teller coupling. A schematic representation based on this splitting scheme is shown in Figure 5(b). The $^2E_{5/2}$ component should maintain the $T_d$ symmetry and still have the $\nu_3(t_2)$ vibrational excitation. This is a stabilization caused by the strong spin-orbit effect against the Jahn-Teller distortion.[6]

Between $P_4^+$ and $Sb_4^+$ is $As_4^+$, which has comparable strengths of spin-orbit and Jahn-Teller effects. The splitting of the $(2t_2)^{-1}$ bands of $As_4^+$ is perhaps better described by scheme (3) with a smaller spin-orbit splitting. With schemes (1) and (3), we may have a better qualitative understanding of the $(2t_2)^{-1}$ bands of the group V tetramer cations. In either case, strong Jahn-Teller splitting or strong spin-orbit splitting, we would expect the $^2T_2$ state to be split into three levels. With reference to Figure 5, Franck-Condon transitions from the neutral ground state to the three final split levels would yield photoelectron spectra as those observed experimentally.

### *C. The $(1a_1)^{-1}$ Bands: Franck-Condon Analyses*

The $^2A_1$ states of $P_4^+$, $As_4^+$, and $Sb_4^+$ are not spatially degenerate, and are not subject to Jahn-Teller or spin-orbit splitting. A single band system is observed in each case. Discrete vibrational structure is resolved in the $P_4^+$ and $As_4^+$ cases, for which the IPs are given in Tables 2 and 3, respectively. From the vibrational spacings, it is clear that the $\nu_1$ mode is excited in each case, as expected. In addition, some hot band transitions due to thermal populations of vibrationally excited neutral molecules are resolved.

The $\nu_1$ vibrational mode involves the stretching motions of the four atoms in phase and maintains the symmetry of the molecule. Therefore, one should be able to evaluate the bond length change from the observed vibrational spectrum with a simple one-dimensional harmonic oscillator. This involves a transformation from the bond stretches to the normal coordinate. This can be conveniently written as:[13]

$$Q_1 = 2\sqrt{m}\, r, \tag{4}$$

where $Q_1$ is the normal coordinate, m is the atomic mass, and r is the bond stretch from the center of the tetrahedral molecule. With Eq. (4), we can calculate the Franck-Condon factors for the $M_4^+$ species at hand, as we have done for diatomics.[14,15] Figures 6 and 7 illustrate the comparison of the theoretical calculations with the experimental spectra. The agreement for $P_4^+$ is excellent while it is only qualitative for $As_4^+$. The vibrational temperatures obtained from these calculations are 450±50 K and 350±50 K for $P_4^+$ and $As_4^+$, respectively.

The bond length for a tetrahedral $M_4$ molecule is measured by $r_{m\text{-}m}$, which has the following relationship with the bond stretch, r, described in the $\nu_1$ vibrational mode as in Eq. (4):

$$r_{m\text{-}m} = 2\left(\sin\frac{109°28'}{2}\right) r \tag{5}$$

The derived $r_{m\text{-}m}$ values from the FCF calculations for $P_4^+$ and $As_4^+$ are given in Table 4, together with the ground state values. The sensitivity in the simulations was ±0.003 Å.

Since only the changes of bond length were obtained in the calculations, the accuracy of $r_{m-m}$ for the ions is ultimately limited by the known ground-state bond lengths.

From the hot-band transitions we can evaluate the vibrational frequency of the ground state. The derived vibrational frequencies for both the neutrals and the cations are also given in Table 4. With reference to Table 2 in Paper II,[1] it is noteworthy that the $\nu_1$ frequency of 360 $cm^{-1}$ obtained from the hot band spectrum of $As_4$ is significantly larger than that derived from earlier measurements using Raman spectroscopy,[16] while that for $P_4$ agrees well with the previous optical measurements.[17] It was difficult to study these species, and, in light of this work, it may be of interest to remeasure their fundamental vibrational frequencies.

### *D. Ionization Thresholds and a Spherical Drop Model for Cluster Electronic Structure*

In Figure 8 are plotted the ionization potentials of the atoms, dimers, and tetramers of the group V elements. The atomic IPs are from Moore's table,[18] the IPs of $N_2$ and $P_2$ are from Ref. 19, the IPs of $As_2$, $Sb_2$, and $Bi_2$ are from Paper I of this study,[20] and the rest are from the current work. It should be kept in mind that the adiabatic IPs for the tetramers are derived from vibronic fits to the experimental spectra.[1]

It is interesting first to consider the trend of the IPs from the atoms to diatomics. We see from Figure 8 that, for N and P, the IP increases upon dimerization, characteristic of valence bonding. However, for As and Sb, the IP decreases for the dimers. For Bi, the diatomic molecule has a higher IP than the atom, which can be largely attributed to the strong relativistic effect in Bi, which causes Bi atom to have an unusually small IP.[21] Therefore, we detect significant changes of chemical bonding, descending the Periodic Table for the group V element, proceeding from covalent bonding to more and more metallic bonding, as expected. As a matter of fact, As, Sb, and Bi are all semimetals.

They are semimetals only because of their rhombohedral crystal lattices. Were they to have simple cubic crystal lattices, they would be very good metals indeed.[22]

Generally for metal clusters, the IP decreases as a function of increasing size, eventually approaching the bulk work function. A classical spherical drop model[23] has been proposed to describe this change of IP as a function of cluster size. The following simple result has been obtained for a small metal droplet:

$$IP(R) = W_\infty + \frac{3}{8}\frac{q^2}{R} \tag{6}$$

where $W_\infty$ is the bulk work function, q is the electron charge, and R is the radius of a cluster. This formula has been shown to describe a number of metal cluster systems to a remarkable degree,[24] including the alkali clusters. In fact, Walstedt and Bell[25] have applied Eq. (6) to Bi clusters and obtained good qualitative agreement with their electron impact ionization data. Recently, Makov et al. have proposed an alternative classical experession for the size dependence of the IPs of spherical clusters:[26]

$$IP(R) = W_\infty + \frac{1}{2}\frac{q^2}{R} \tag{7}$$

It was concluded that Eq. (7) should account better for large clusters, while Eq. (6) should fit well for smaller clusters due to quantum corrections to Eq. (7).

Determination of R for a particular cluster is obviously a difficult task, requiring knowledge of the atomic volume. To first approximation, one could use:

$$R = n^{1/3} r_0 \tag{8}$$

where n is the number of atoms in a cluster, and $r_0$ can be chosen as half of the average bulk atomic separation or half of the diatomic bond length.[24] Using this expression, and the bond lengths from Ref. 19, we have found that Eq. (7) described $As_n$ well while Eq.

(6) fits better with data for $Sb_n$ and $Bi_n$. It was not clear why Eq. (7) should fit better for $As_n$. Obviously, a larger data set would be desirable. The dashed curves in Figure 8 illustrate the calculated IPs of $As_n$, $Sb_n$, and $Bi_n$ for n up to 10, with each curve converging to its bulk work function,[27] when n approaches infinity. It is seen that the IPs of As4, and in particular, Sb4 deviate severely from the model. It should be noted that the Jahn-Teller effect profoundly altered the IPs of the tetramers and lowered the symmetries of the cations. Were there no Jahn-Teller distortions in the cations, the IPs of the tetramers would have much better agreement with the model. Therefore, the agreement with the experimental IPs should still be regarded to be gratifying given the limited experimental data, and the approximate nature of the model.

## V. Conclusions

The high resolution PE spectra of the tetramers of the group V elements have been obtained. Vibrational structure in the $\nu_1(a_1)$ mode is fully resolved for $P_4^+$ and $As_4^+$ in the $^2A_1$ states, which enabled us to carry out Franck-Condon factor calculations for the $^2A_1$ states and obtain the bond length changes in the $^2A_1$ states of the two cationic species. From our Franck-Condon factor fitting, the $\nu_1$ vibrational frequency of $As_4$ reported before has been found to be too small.

The $^2E$ states of all three tetramers, $P_4^+$, $As_4^+$, and $Sb_4^+$, are found to undergo strong Jahn-Teller distortions, coupled with the $\nu_2(e)$ vibrational mode and split into two spectral bands. Partially resolved vibrational structure in the $P_4^+$ spectrum is consistent with the excitation of the $\nu_2$ (e) mode. Both Jahn-Teller and spin-orbit effects were shown to play important roles in the $^2T_2$ states of the tetramers. The spin-orbit effect is dominant in the case of $Sb_4^+$, while the Jahn-Teller effect is dominant in $P_4^+$. From the resolved vibrational structure in the $^2T_2$ state of $P_4^+$, the $\nu_3(t_2)$ vibrational mode was found to be the one which is principally active in the Jahn-Teller coupling.

A classical metal droplet model fits trends in the ionization potentials of the clusters as a function of size. The model is shown to work reasonably well, although a larger data set with larger cluster sizes would be desirable.

## Acknowledgment

DAS thanks the Alexander von Humboldt Foundation for support through a Senior Scientist Award, and Professors G. Kaindl and E. Mattias for their hospitality during his stay in FB Physik, FU Berlin. This work was supported by the Director, Office of Energy Research, Office of Basic Energy Sciences, Chemical Sciences Division of the U.S. Department of Energy under Contract No. DE-AC03-76SF00098. Theoretical contributions by EG and ERG were supported by the National Science Foundation through Grant No. CHE-8920555.

## References


1. L.S. Wang, B. Niu, Y.T. Lee, D.A. Shirley, A. Ghelichkhani, and E.R. Grant, part II, (in preparation).
2. H.A. Jahn and E. Teller, *Proc. Roy. Soc.* **A161**, 220 (1937).
3. G. Herzberg, *Molecular Spectra and Molecular Structure III. Electronic Spectra and Electronic Structure of Polyatomic Molecules* (Van Nostrand Reinhold, New York, 1966).
4. R. L. Whetten, G. S. Ezra and E. R. Grant, *Annu. Rev. Phys. Chem.* **36**, 277 (1985).
5. (a) I.B. Bersuker, *The Jahn-Teller Effect and Vibronic Interactions in Modern Chemistry* (Plenum Press, New York, 1984); (b) U. Opik and M.H.L. Pryce, *Proc. Roy. Soc.* **A238**, 425 (1957); (c) H.C. Longuet-Higgins, U. Opik, M.H.L. Pryce, and R.A. Sack, *Proc. Roy. Soc.* **A244**, 1 (1958); (d) H.C. Longuet-Higgins, *Adv. Spectrosc.* **2**, 429 (1961); (e)B.R. Judd, *Adv. Chem. Phys.* **57**, 247 (1984); (f) H. Koppel, W. Domcke, and L.S. Cederbaum, *Adv. Chem. Phys.* **57**, 59 (1984).
6. (a) M. Wagner, *Z. Phys.* **230**, 460 (1970); (b) M.D. Sturge, *Solid State Phys.* **20**, 91 (1967).
7. (a) D.P. DiLella, K.V. Taylor, and M. Moskovits, *J. Phys. Chem.* **87**, 524 (1983); (b) M.D. Morse, J.B. Hopkins, P.R.R. Langridge-Smith, and R.E. Smalley, *J. Chem. Phys.* **79**, 5316 (1983); (c) T.C. Thompson, D.G. Truhlar, and C.A. Mead, *J. Chem. Phys.* **82**, 2392 (1985); (d) W.H. Crumley, J.S. Hayden, and J.L. Gole, *J. Chem. Phys.* **84**, 5250 (1986).
8. (a) A. Herrmann, M. Hofmann, S. Leutwyler, E. Schumacher, and L. Woste, *Chem. Phys. Lett.* **62**, 216 (1979); (b) J.L. Gole, G.J. Green, S.A. Pace, and D.R. Preuss, *J. Chem. Phys.* **76**, 2247 (1982); (c) S.C. Ritchtsmeler, M.L. Hendewerk, D.A. Dixon, and J.L. Gole, *J. Phys. Chem.*, **86**, 3932 (1982); (d) M. Broyer, G.

Delacretaz, P. Labastie, J.P.Wolf, and L. Woste, *Phys. Rev. Lett.* **57**, 1851 (1986); (e) M. Broyer, G. Delacretaz, G.Q. Ni, R.L. Whetten, J.P. Wolf, and L. Woste, *Phys. Rev. Lett.*, **62**, 2100 (1989).

9. (a) W.H. Gerber and E. Schumacher, *J. Chem. Phys.* **69**, 1692 (1978); (b) J.L. Gole, R.H. Childs, D.A. Dixon, and R.A. Eades, *J. Chem. Phys.* **72**, 6368 (1980); (c) R.A. Eades, M.L. Hendewerk, R. Frey, D.A. Dixon, and J.L. Gole, *J. Chem. Phys.* **76**, 3075 (1982); (d) J.L. Martins, R. Car, and J. Buttet, *J. Chem. Phys.* **78**, 5646 (1983); (e) T.C. Thompson, G. Izmirlian, Jr., S.J. Lemon, D.G. Truhlar, and C. A. Mead, *J. Chem. Phys.* **82**, 5597 (1985); (f) J.D. Wolf, G. Delacretaz, and L. Woste, *Phys. Rev. Lett.* **63**, 1946 (1989).
10. F.S. Ham, *Phys. Rev.* **A138**, 1727 (1965).
11. J.H. Van Vleck, *Physica* **26**, 544 (1960).
12. H. Koppel, private communication.
13. G. Herzberg, *Molecular Spectra and Molecular Structure II. Infrared and Raman Spectra of Polyatomic Molecules* (Van Nostrand Reinhold, New York, 1945).
14. L.S. Wang, Y.T. Lee, D.A. Shirley, K. Balasubramanian, and P. Feng, Part I, (in preparation).
15. (a) L.S. Wang, B. Niu, Y.T. Lee, and D.A. Shirley, *Chem. Phys. Lett.* **158**, 297 (1989); (b) L.S. Wang, B. Niu, Y.T. Lee, D.A. Shirley, and K. Balasubramanian, *J. Chem. Phys.* **92**, 899 (1990).
16. S.B. Brumbach and G.M. Rosenblatt, *J. Chem. Phys.* **56**, 3110 (1972).
17. H.S. Gutowsky and L.J. Hoffman, *J. Am. Chem. Soc.* **72**, 5751 (1950).
18. C.E. Moore, *Tables of Atomic Energy Levels* (U.S. National Bureau of Standards, Washington D.C., 1971).
19. K.P. Huber and G. Herzberg, *Molecular Spectra and Molecular Structure IV. Constants of Diatomic Molecules* (Van Nostrand Reinhold, New York, 1979).

20. L.S. Wang, Y.T. Lee, D.A. Shirley, K. Balasubramanian, and P. Feng, Part I, (in preparation).

21. P. Pyykko, *Chem. Rev.* **88**, 563 (1988).

22. N.W. Ashcroft and N.D. Mermin, *Solid State Physics* (Saunders College, Philadelphia, 1976).

23. D.M. Wood, *Phys. Rev. Lett.* **46**, 749 (1981).

24. (a) M.M. Kappes, M. Schar, P. Radi, and E. Schumacher, *J. Chem. Phys.* **84**, 1863 (1986); (b) D.G. Leopold, J. Ho, and W.C. Lineberger, *J. Chem. Phys.* **86**, 1715 (1987).

25. R.E. Walstedt and R.F. Bell, *Phys. Rev.* **A33**, 2830 (1986).

26. G. Makov, A. Nitzan, and L.E. Brus, *J. Chem. Phys.* **88**, 5076 (1988).

27. R.C. Weast, M.J. Astle, and W.H. Beyer, Eds., *CRC Handbook of Chemistry and Physics,* 67th edition (CRC Press, Boca Raton, 1986).

28. G. Trinquier, J.P. Malrieu, and J.P. Dandey, *Chem. Phys. Lett.* **80**, 552 (1981).

Table 1. Ionization potentials (IP) and the observed vibrational spacings (VS) in the PE spectra of $P_4$, $As_4$, and $Sb_4$.

| | | IPa (eV)[a] | IPv (eV)[b] | VS ($cm^{-1}$) |
|---|---|---|---|---|
| $P_4$ | $(1e)^{-1}$ | 8.95 | 9.46(1) | 315(10) |
| | | | 9.92(1) | 275(10) |
| | $(2t_2)^{-1}$ | 10.1 | 10.36(1) | 400(10) |
| | | | 10.53(1) | (370) |
| | | | 10.72(2) | |
| | $(2a_1)^{-1}$ | 11.776(3) | 11.847(3) | 577(5) |
| $As_4$ | $(1e)^{-1}$ | 7.83 | 8.75(1) | |
| | | | 9.16(1) | |
| | $(2t_2)^{-1}$ | 9.5 | 9.76(2) | (240) |
| | | | 9.97(1) | (290) |
| | | | 10.11(3) | |
| | $(2a_1)^{-1}$ | 11.017(3) | 11.058(3) | 350(6) |
| $Sb_4$ | $(1e)^{-1}$ | 6.61 | 7.85(1) | |
| | | | 8.27(1) | |
| | $(2t_2)^{-1}$ | 8.5 | 8.69(1) | |
| | | | 9.09(1) | |
| | | | 9.22(3) | |
| | $(2a_1)^{-1}$ | 9.8 | 9.89(1) | |

a. Adiabatic IP established in the case of $(1e)^{-1}$ by Jahn-Teller spectral simulation, as discussed in Ref. 1. .

b. Vertical IP.

Table 2. Ionization potentials (IP) and assignments of the $P_4^+ {}^2A_1$ state.

| IP (eV) | Interval (meV) | v ($\nu_1$)[a] |
|---|---|---|
| 11.700(3) | | Hot band (1→0) |
| 11.777(3) | 77 | 0 |
| 11.847(3) | 70 | 1 |
| 11.916(3) | 69 | 2 |
| 11.985(3) | 69 | 3 |
| 12.053(4) | 68 | 4 |
| 12.121(4) | 68 | 5 |

a. Vibrational quanta of the $\nu_1$ mode.

Table 3. Ionization potentials and assignments of the $As_4^+$ $^2A_1$ state.

| IP (eV) | Interval (meV) | v ($\nu_1$)[a] |
|---|---|---|
| 10.929(3) | | Hot band (2→0) |
| 10.973(3) | 44 | Hot band (1→0) |
| 11.017(3) | 44 | 0 |
| 11.058(3) | 41 | 1 |
| 11.098(3) | 40 | 2 |
| 11.138(3) | 40 | 3 |
| 11.175(4) | 37 | 4 |
| 11.210(5) | 35 | 5 |

a. Vibrational quanta of the $\nu_1$ mode.

Table 4. Spectroscopic constants of the $^2A_1$ states of $P_4^+$ and $As_4^+$.

| | | $\omega_e$ ($\nu_1$) ($cm^{-1}$) [a] | $r_{m-m}$ (Å) [b] |
|---|---|---|---|
| $P_4$ | $^1A_1$ | 610(10) [c] | 2.21 [d] |
| $P_4^+$ | $^2A_1$ | 577(5) [c] | 2.264 [e] |
| $As_4$ | $^1A_1$ | 360(6) [c] | 2.435 [d] |
| $As_4^+$ | $^2A_1$ | 350(6) [c] | 2.495 [f] |

a. Vibrational frequency of the $\nu_1$ mode.

b. Equilibrium bond distance between two atoms.

c. From this work.

d. From Ref. 28.

e. Franck-Condon factor calculations yielded the change of $r_{m-m}$, which was 0.054 ± 0.003 Å.

f. Franck-Condon factor calculations yielded the change of $r_{m-m}$, which was 0.060 ± 0.003 Å.

## Figure Captions

Figure 1 The $(1e)^{-1}$ and $(2t_2)^{-1}$ bands of the $P_4^+$ spectrum. Three Voigt functions are drawn to show the three components in the $(2t_2)^{-1}$ bands.

Figure 2 The $(1e)^{-1}$ and $(2t_2)^{-1}$ bands of the $As_4^+$ spectrum. Three Voigt functions are drawn to show the three components in the $(2t_2)^{-1}$ bands.

Figure 3 The $(1e)^{-1}$ and $(2t_2)^{-1}$ bands of the $Sb_4^+$ spectrum. Three Voigt functions are drawn to show the three components in the $(2t_2)^{-1}$ bands.

Figure 4 A schematic configuration-coordinate diagram for the transitions from a nondegenerate ground state to a Jahn-Teller active doubly degenerate state in a $T_d$ molecule. It is, in fact, a section through a three-dimensional diagram (see Ref. 1) that has a cylindrical symmetry in a harmonic approximation.

Figure 5 Schematic configuration-coordinate diagrams showing the transitions from a nondegenerate ground state to a Jahn-Teller split $^2T_2$ state of a tetrahedral $M_4$ molecule coupled with the $\nu_3(t_2)$ vibrations: (a) zero spin-orbit splitting; (b) strong spin-orbit splitting.

Figure 6 Comparison of calculated Franck-Condon factors with the experiment of $P_4^+$ $^2A_1$ state. (— theoretical, ..... experimental).

Figure 7 Comparison of calculated Franck-Condon factors with the experiment of $As_4^+$ $^2A_1$ state. (— theoretical, ..... experimental).

Figure 8 Ionization potentials as a function of cluster size for the group V elements. (— experimental, - - - theoretical).

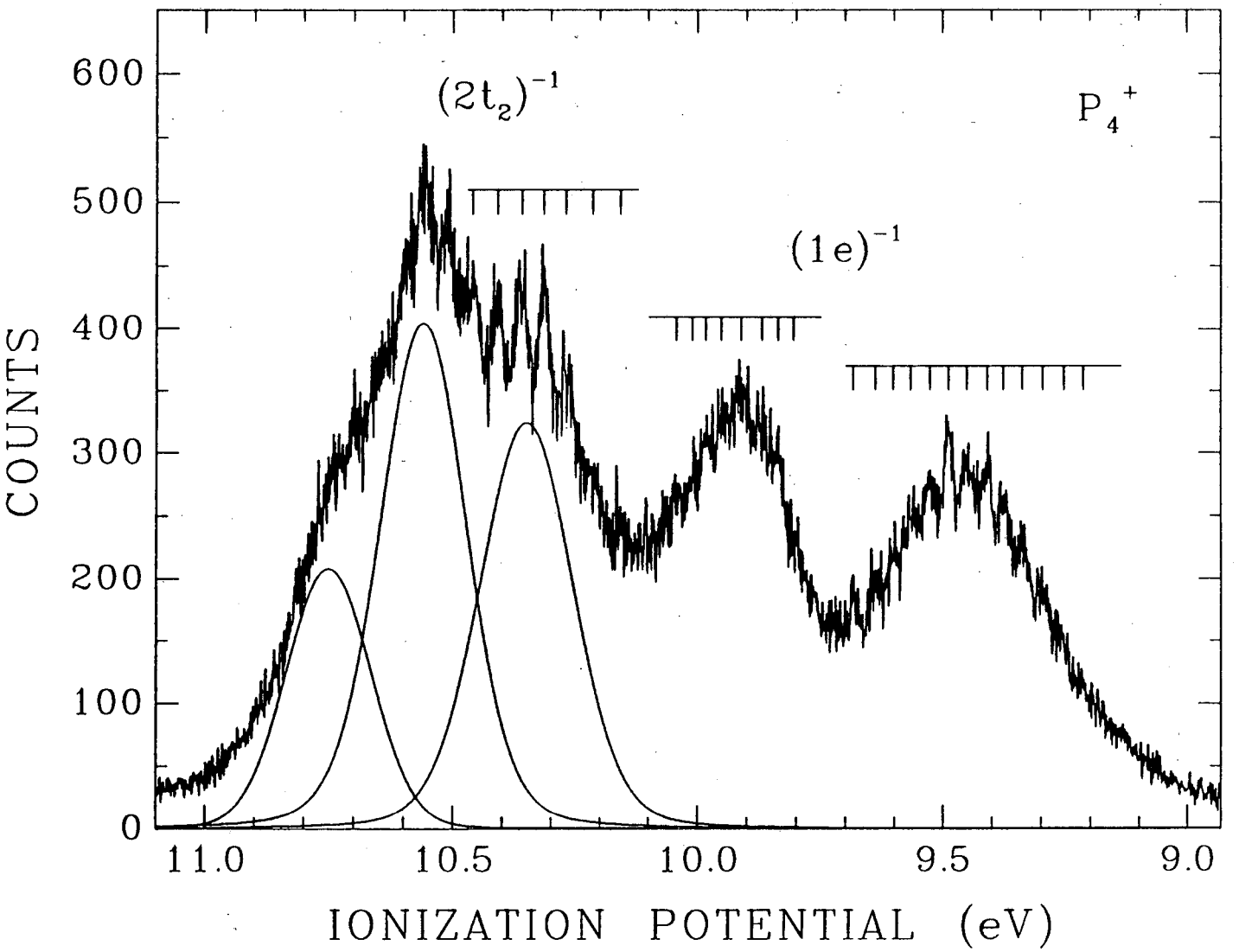
600
500
400
300
200
100
0
COUNTS
$(2t_2)^{-1}$
$(1e)^{-1}$
$P_4^+$
11.0
10.5
10.0
9.5
9.0
IONIZATION POTENTIAL (eV)
XBL 902-407

Figure 1

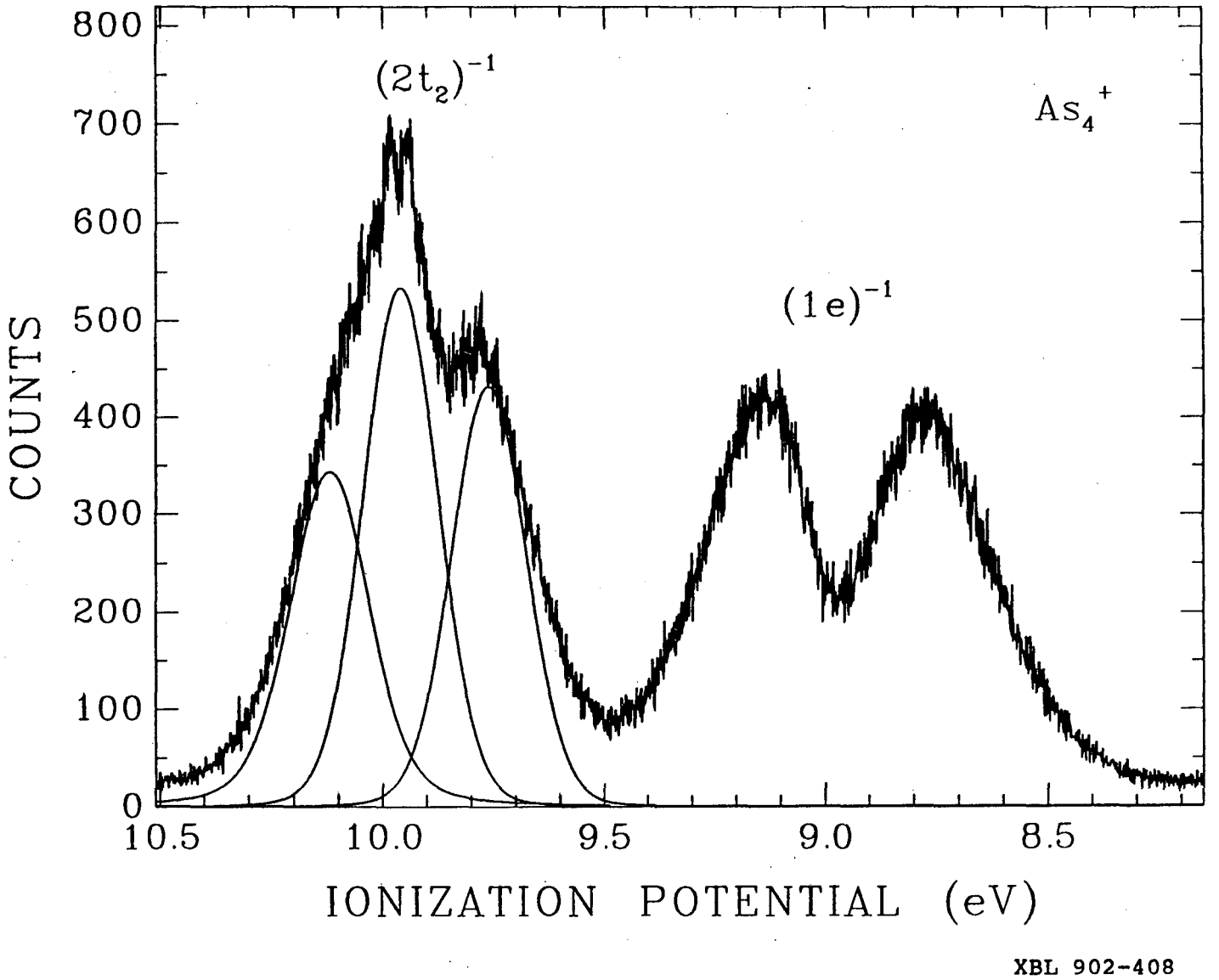
800
700
600
500
400
300
200
100
0
COUNTS
$(2t_2)^{-1}$
$(1e)^{-1}$
$As_4^+$
10.5
10.0
9.5
9.0
8.5
IONIZATION POTENTIAL (eV)
XBL 902-408

Figure 2

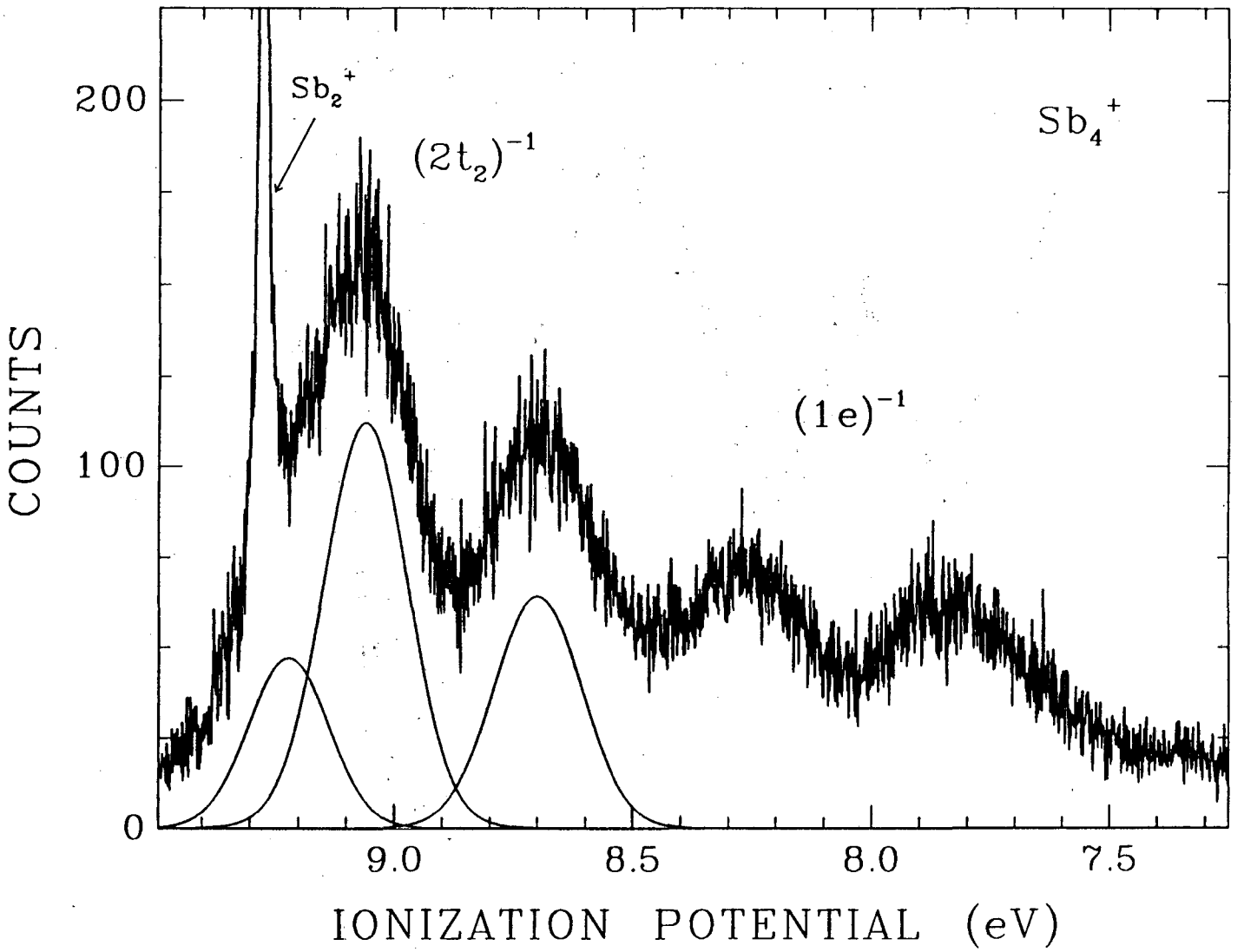
200
100
0
COUNTS
$Sb_2^+$
$(2t_2)^{-1}$
$Sb_4^+$
$(1e)^{-1}$
9.0
8.5
8.0
7.5
IONIZATION POTENTIAL (eV)
XBL 902-409

Figure 3

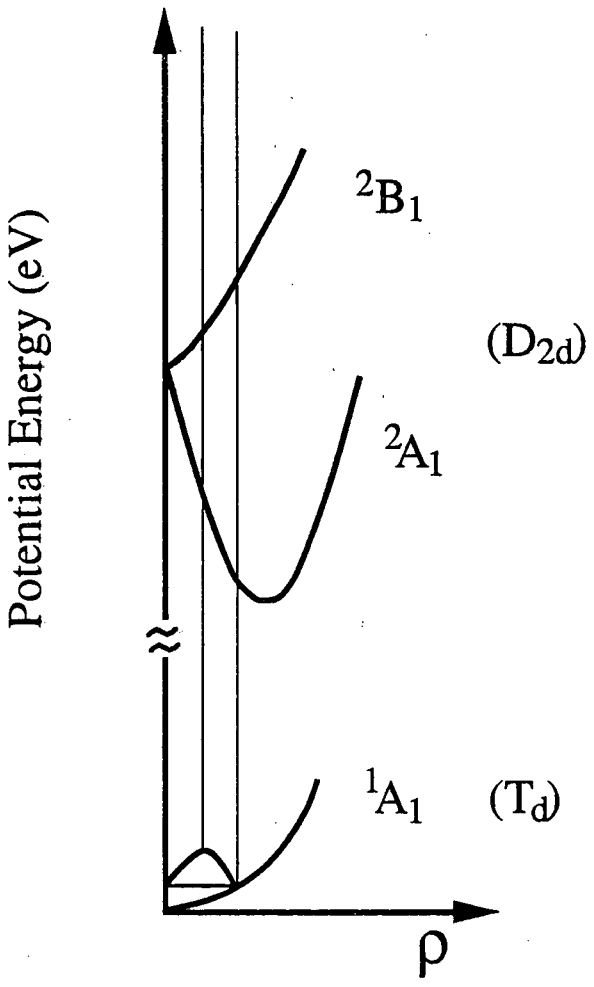


Figure 4

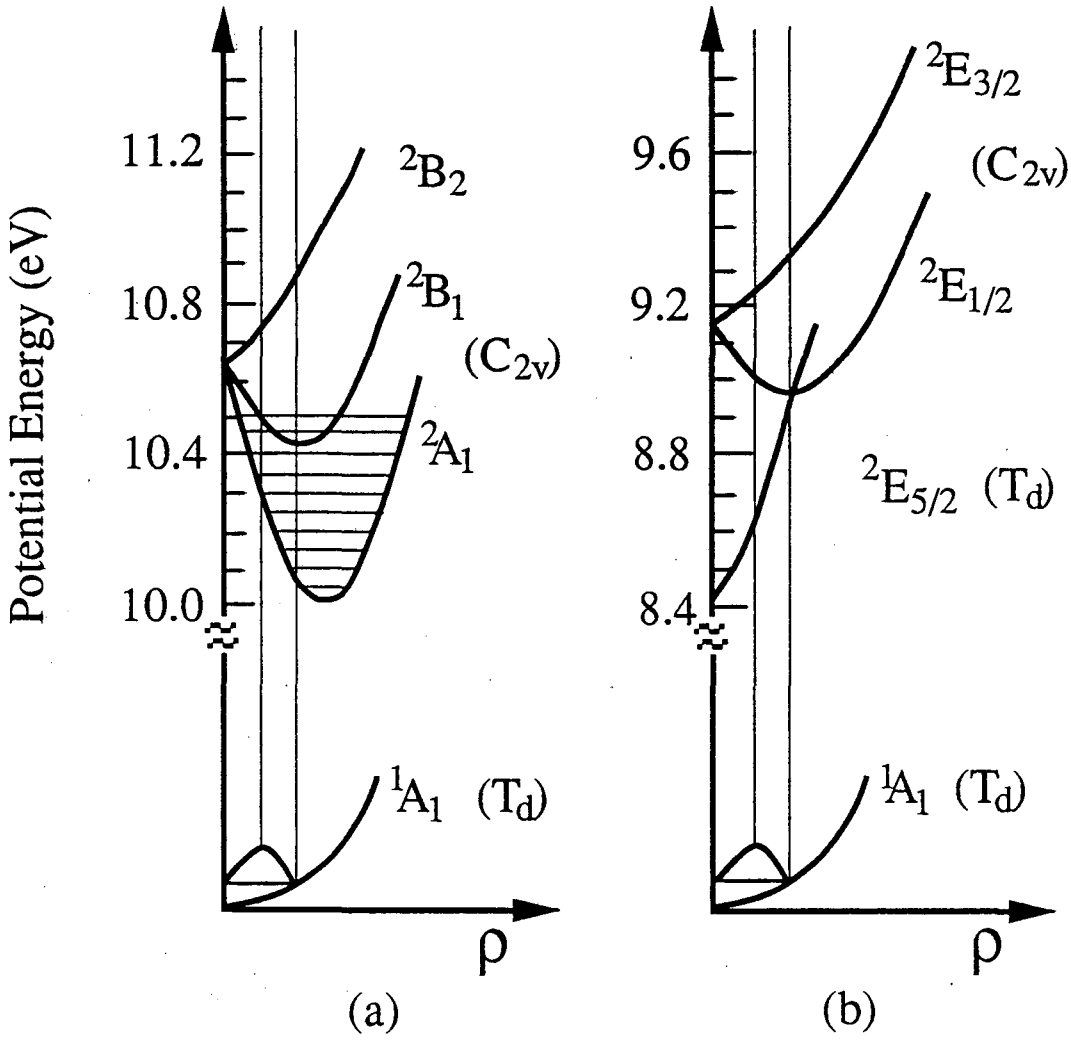
Potential Energy (eV)
11.2
10.8
10.4
10.0
$^2B_2$
$^2B_1$
$(C_{2v})$
$^2A_1$
$^1A_1$ $(T_d)$
ρ
(a)
9.6
9.2
8.8
8.4
$^2E_{3/2}$
$(C_{2v})$
$^2E_{1/2}$
$^2E_{5/2}$ $(T_d)$
$^1A_1$ $(T_d)$
ρ
(b)

Figure 5

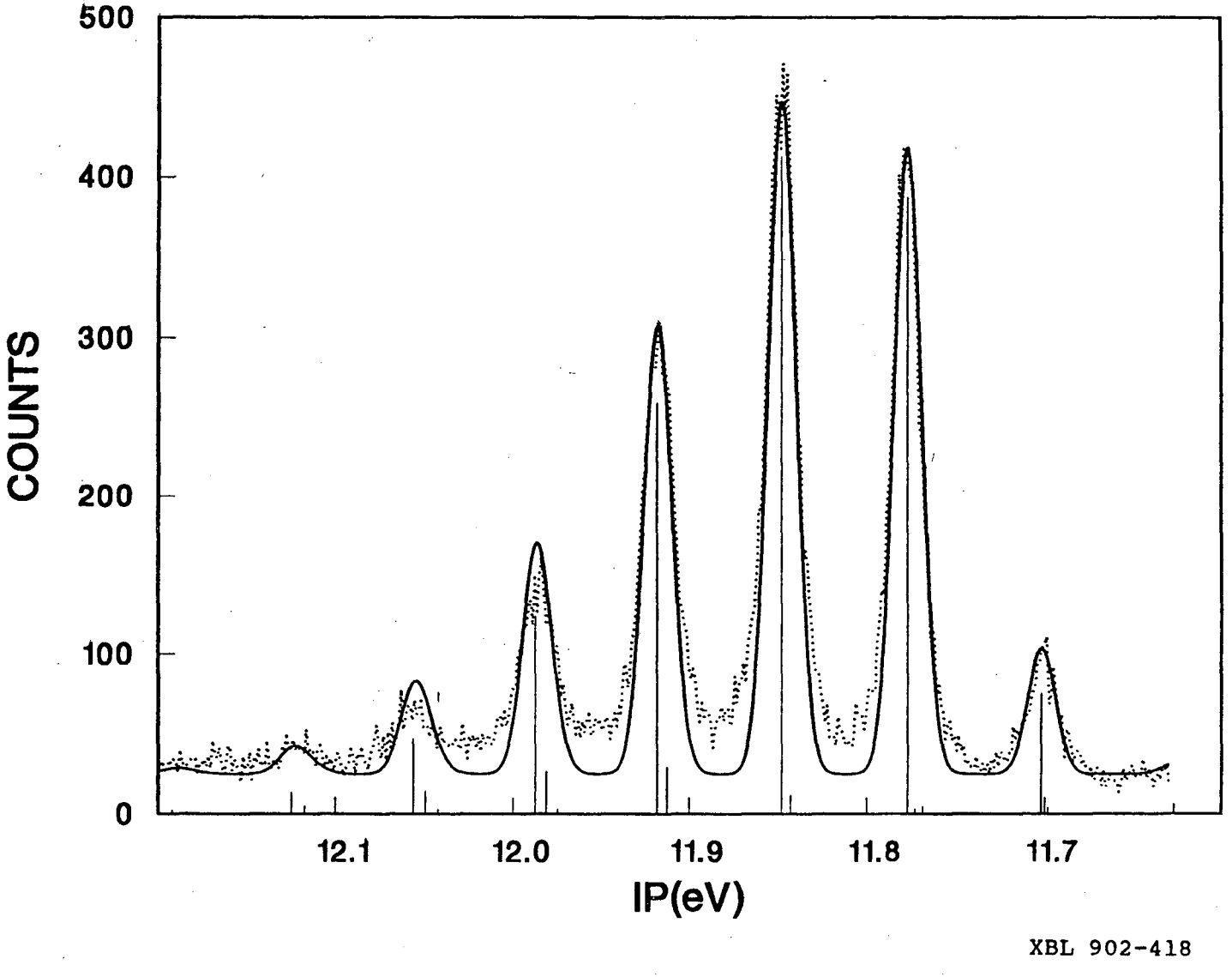
500
400
300
200
100
0
COUNTS
12.1
12.0
11.9
11.8
11.7
IP(eV)
XBL 902-418

Figure 6

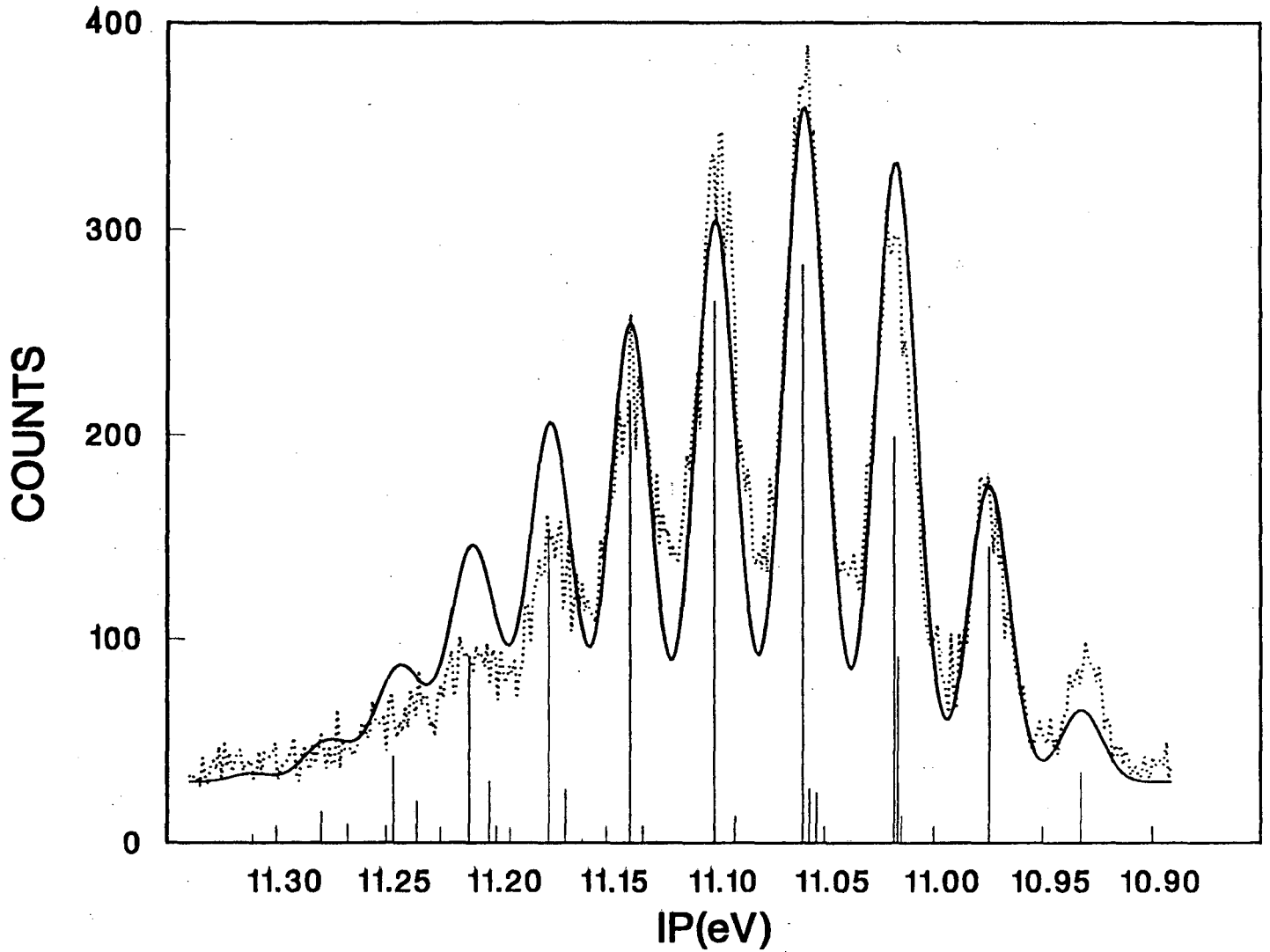
400
300
200
100
0
COUNTS
11.30
11.25
11.20
11.15
11.10
11.05
11.00
10.95
10.90
IP(eV)
XBL 902-419

Figure 7

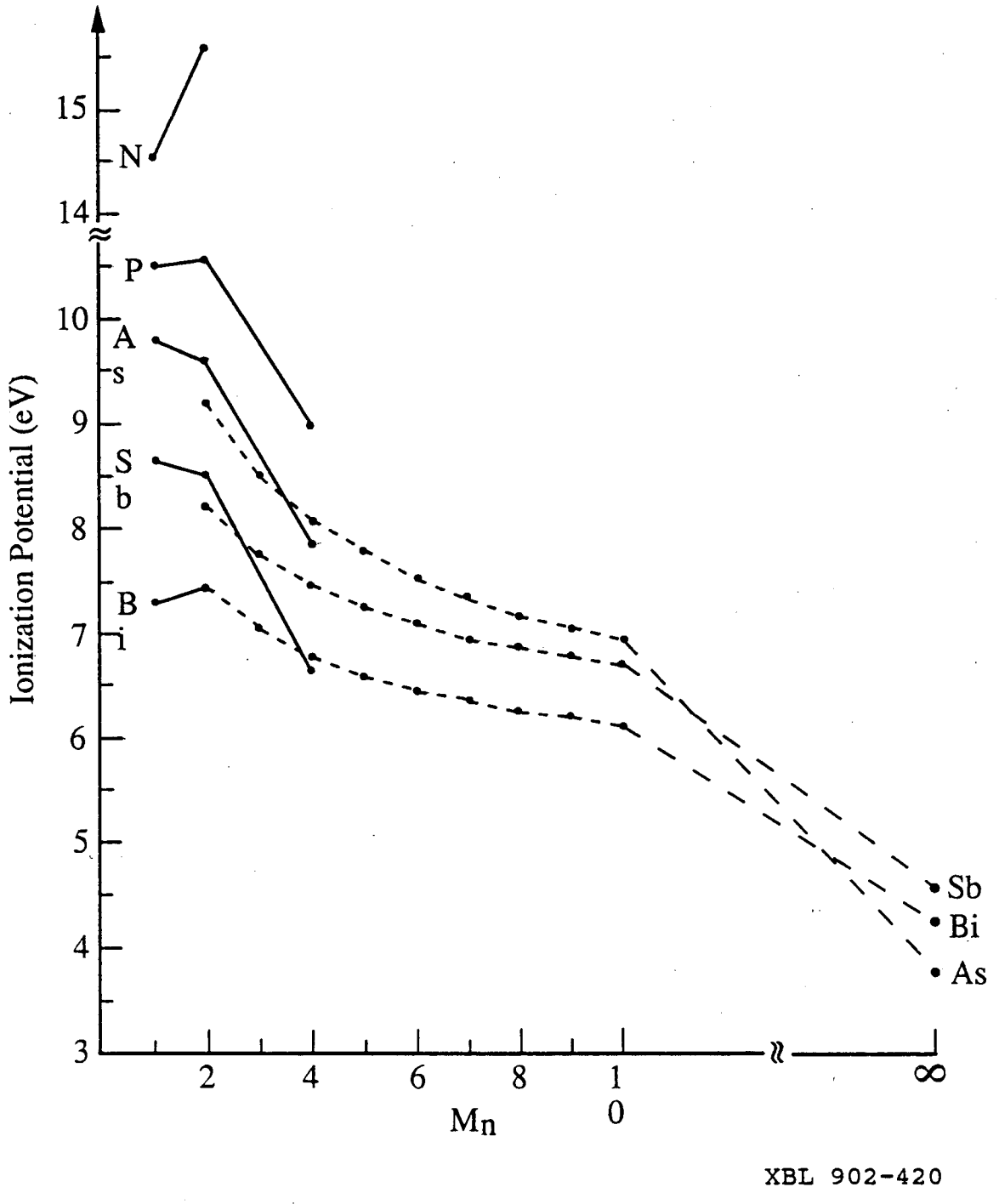
Ionization Potential (eV)
15
14
10
9
8
7
6
5
4
3
N
P
As
Sb
Bi
B
i
2
4
6
8
1
0
∞
Mn
XBL 902-420

Figure 8

LAWRENCE BERKELEY LABORATORY
UNIVERSITY OF CALIFORNIA
INFORMATION RESOURCES DEPARTMENT
BERKELEY, CALIFORNIA 94720